Supplementary Material for

Upcycling plastic wastes into high-performance nano-MOFs by efficient neutral hydrolysis for water adsorption and photocatalysis

*Ling-Xia Yun[a,b], Meng Qiao[a,b], Bin Zhang[a,b], Hang-Tian Zhang[c], Jie-Xin Wang[a,b]**

[a]State Key Laboratory of Organic-Inorganic Composites, Beijing University of Chemical Technology, Beijing 100029, PR China;

[b]Research Center of the Ministry of Education for High Gravity Engineering and Technology, Beijings University of Chemical Technology, Beijing, 100029, PR China

[c]Quzhou Innovation Institute for Chemical Engineering and Materials, Quzhou, Zhejiang 324000, PR China

*Corresponding authors. E-mails: wangjx@mail.buct.edu.cn (Jie-Xin Wang)

1. Details of experimental procedure

1.1. PET hydrolysis

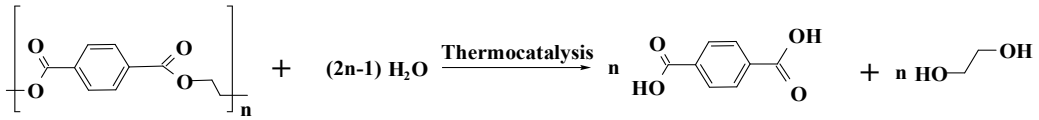

PET TPA (S1)

The pseudo-first-order kinetics are calculated as follows (Equation S4-S6), where C_t and C_0 refer to the solid contents of PET at different times; X refers to PET conversion; k is the apparent rate constant; E_a refers to the apparent activation energy. A, R, and T refer to the pre-exponential factor, gas constant (8.314 $J \cdot k^{-1} \cdot mol^{-1}$), and reaction temperature in Kelvin, respectively.

$$\ln(C_t / C_0) = \ln(1 - X) \tag{S2}$$

$$\ln(1 - X) = -kt \tag{S3}$$

$$\ln k = -\frac{E_a}{RT} + \ln A \tag{S4}$$

1.2. Raw materials and MOF synthesis

All the reagents and solvents were commercially available and directly used without additional purification. Chromium(III) nitrate nonahydrate ($Cr(NO_3)_3 \cdot 9H_2O$, >99%), zirconium chloride ($ZrCl_4$, >99%), cerium (IV) ammonium nitrate ($(NH_4)_2Ce(NO_3)_6$, 99%), and iron(III) chloride hexahydrate ($FeCl_3 \cdot 6H_2O$, >99%) were purchased from Aladdin (Shanghai, China). Aluminum nitrate nonahydrate ($Al(NO_3)_3 \cdot 9H_2O$, >99%) was purchased from Macklin (Shanghai, China).

1.2.1. One-Pot synthesis

One-pot synthesis of MOFs was directly performed after PET wastes were completely hydrolyzed to terephthalic acid as follows (Scheme 1).

Synthesis of OP-MIL-101 (Cr): 0.453 g PET was catalytically hydrolyzed by 0.0045 g ZnO nanoparticles in 5 mL water. Then 1.060 g $Cr(NO_3)_3 \cdot 9H_2O$ dispersed in

75 mL water was introduced in the hydrolysate slurry, followed by 6 h of heating at 180 ℃ in a Teflon liner placed in an oven.

Synthesis of OP-MIL-53(Al): 0.599 g PET was catalytically hydrolyzed by 0.0060 g ZnO nanoparticles in 8 mL water. Then 1.310 g $Al(NO_3)_3 \cdot 9H_2O$ dispersed in 32 mL DMF was added to the hydrolysate slurry, followed by 12 h of heating at 150 ℃ in a Teflon liner placed in an oven.

Synthesis of OP-MIL-53(Al, Fe): 0.599 g PET was catalytically hydrolyzed by 0.0060 g ZnO nanoparticles in 8 mL water. Then 0.788 g $Al(NO_3)_3 \cdot 9H_2O$ and 0.379 g $FeCl_3 \cdot 6H_2O$ dispersed in 32 mL DMF was added to the hydrolysate slurry, followed by 12 h of heating at 150 ℃ in a Teflon liner placed in an oven.

Synthesis of OP-UiO-66(Zr): 0.663 g PET was catalytically hydrolyzed by 0.0066 g ZnO nanoparticles in 10 mL water. Then 0.480 g $ZrCl_4$ dispersed in 40 mL DMF was added to the hydrolysate slurry. The system was heated to 120 ℃ at a rate of 1 ℃/min and held at 120 ℃ for 24 h in a Teflon liner placed in an oven.

Synthesis of OP-UiO-66(Ce): 0.855 g PET was catalytically hydrolyzed by 0.0086 g ZnO nanoparticles in 10 mL water. Then 2.741 g $(NH_4)_2Ce(NO_3)_6$ dispersed in 40 mL DMF was added to the hydrolysate slurry, followed by 0.5 h of heating at 110 ℃ in a Teflon liner placed in an oven.

The OP-MOF products were collected by centrifugation, washed with MeOH and DMF, and finally dried under vacuum. Except ZnO loaded on OP-MOFs, other ZnO nanoparticles highly dispersed in water are recycled by the centrifugation after MOF synthesis.

1.2.2. Two-Pot synthesis

Two-pot synthesis of MOFs was performed after PET wastes were completely hydrolyzed, and then TPA powders were obtained by the process of alkalization (3.5 g KOH, after hydrolysis of 6 g PET), then acidification (6.34 g chlorhydric acid, 36 wt%), and subsequent centrifugation and drying. The terephthalic acid powders stepwisely prepared by the hydrolysis were used instead of TPA slurry in one-pot synthesis. The

amount of terephthalic acid powders used to prepare **TP-MIL-101 (Cr), TP-MIL-53(Al), TP-MIL-53(Al, Fe), TP-UiO-66(Zr),** and **TP-UiO-66(Ce)** were 0.440 g, 0.582 g, 0.582 g, 0.644 g, and 0.830 g, respectively. The ratios of metal to the ligand and solvothermal procedures of the above MOFs were determined according to some references[1-5].

1.3. Structural characterizations

The thermal stability of the material was characterized using a thermogravimetric Mettler TGA2 analyzer (under a nitrogen atmosphere, the heating rate is 10 ℃/min, and a test range from 30 to 800 ℃). The morphology and particle sizes of the sample were characterized by a Hitachi 7700 scanning electron microscope. The ^{1}H NMR spectra were analyzed by BRUKER AVANCE 400. Fourier-transformed infrared spectroscopy (FTIR) was conducted on a Nicolet iS5 spectrometer. X-ray photoelectron spectroscopy (XPS) was examined with a Thermo Scientific K-Alpha. Inductively coupled plasma (ICP) examinations were carried out by Shimadzu ICPE-9000 (OES).

2. Material characterization

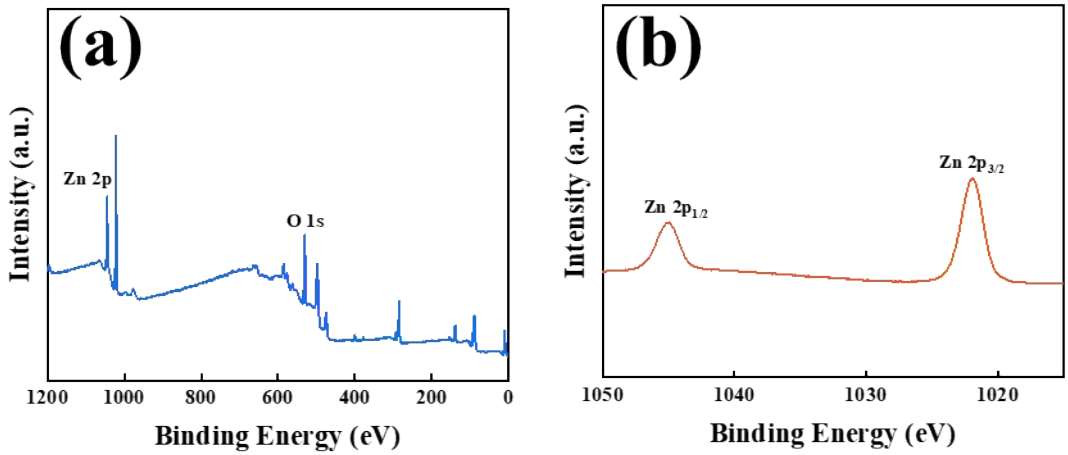

Figure S1. (a, b) XPS spectra of the ZnO nanoparticles.

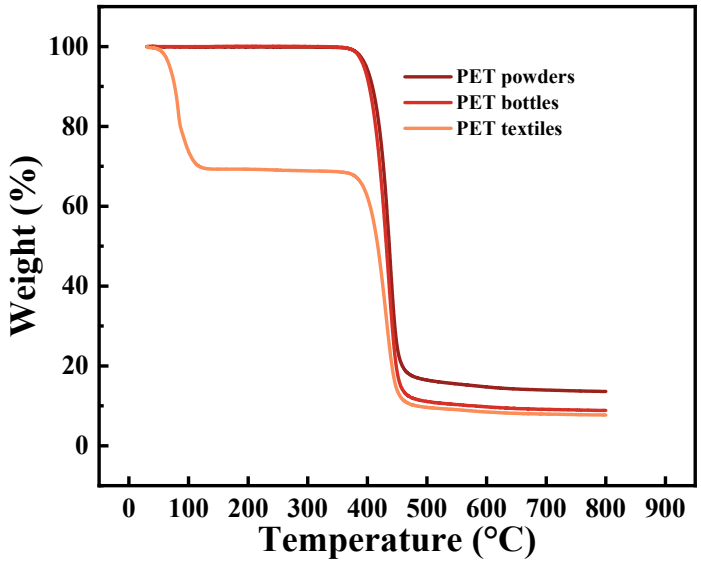

Figure S2. TG curves of PET samples.

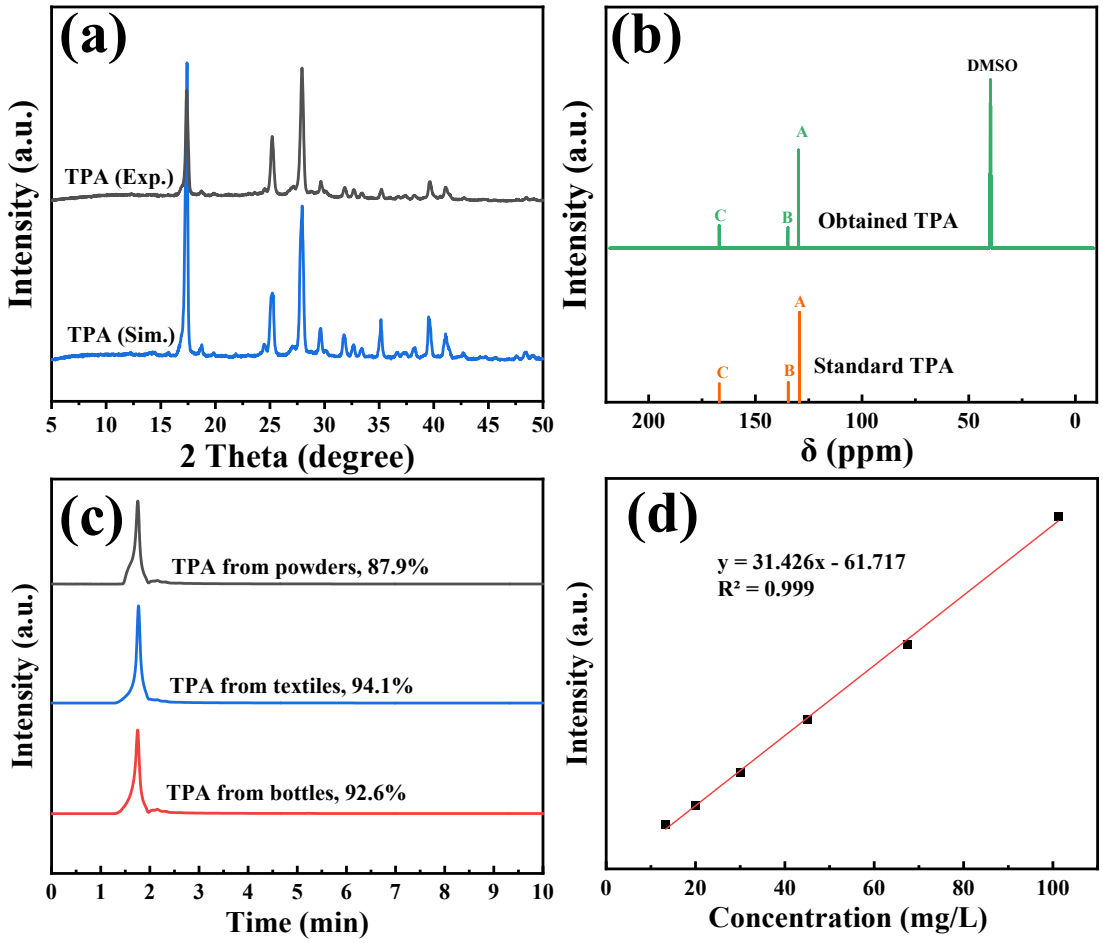

Figure S3. (a) XRD patterns and (b) ^{13}C NMR spectra of the PET powders-derived TPA and standard TPA. (c) HPLC chromatograms of the PET-derived TPA. (d) The corresponding

calibration curve of standard TPA used to quantify the purities of the produced TPA.

To compares the performances of the synthesized NPs with some reported catalysts, the related weight hourly space velocity (WHSV) for the hydrolysis reaction are calculated using the following equation:

$$\mathrm{WHSV} = \frac{m_{product}}{m_{catalyst} \times t} \tag{S5}$$

where $m_{product}$ and $m_{catalyst}$ represent the weight of the product and the catalyst respectively, and t is the reaction time. The reaction temperature was included in the diagram as an important factor.

Table S1. Comparison of reported PET hydrolysis processes.

Reaction	Catalyst	Mass ratio of cat./PET (%)	Mass ratio of solvent/ PET	Temperature (°C)	Time (h)	Product yield (%)	Ref.	WHSV ($g_{TPA} \cdot g_{cat}^{-1} \cdot h^{-1}$)
Neutral hydrolysis	ZnO aqueous nanodispersion	1	10	200	1	95	**this work**	82.1
	ZSM-5 acidic catalyst	50	119	200 (microwave assisted)	0.5	90	6	3.1
	TPA	80	8	220	3	95.5	7	0.3
	$Ni/\gamma\text{-}Al_2O_3$	12.9	10	267	0.8	97.1	8	8.1
	$[HSO_3\text{-}pmim][HSO_4]$	1.3	220	170	4.5	88	9	13.0
Uncatalyzed	-	0	10	200	2	<4	10	-
	-	0	2.85	200	24	97.7	11	-
acid hydrolysis	p-toluenesulfonic acid	16	20	150	1.5	96.2	12	3.5
	Poly (4-styrenesulfonic acid)	0.1	50	150	14	~55	13	34.0

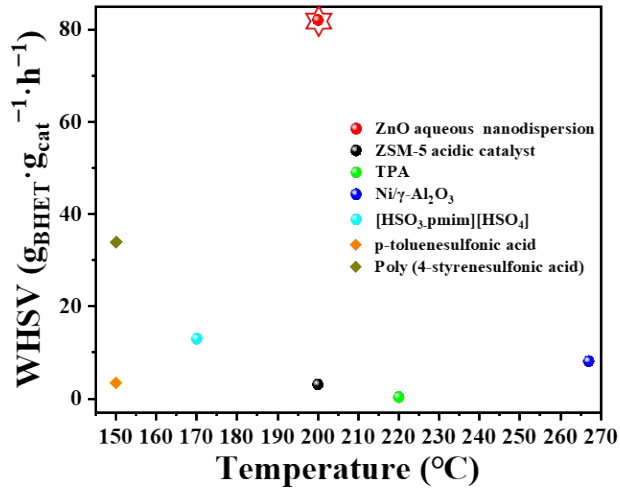

Figure S4. Comparison of reported catalysts for neutral hydrolysis (spheres) and acid hydrolysis (diamonds).

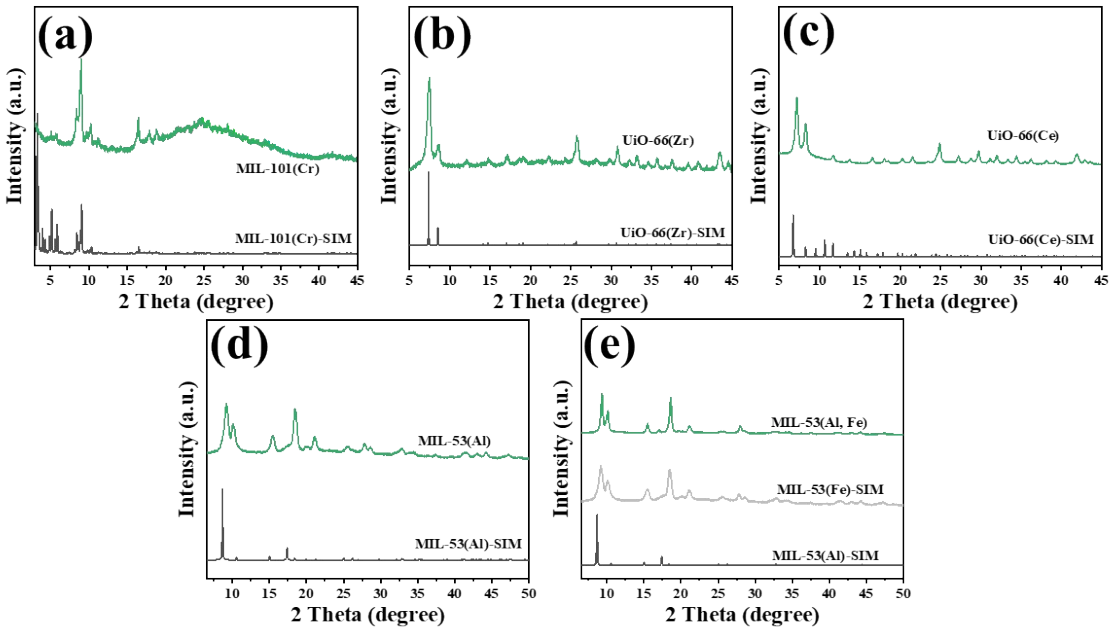

Figure S5. PXRD patterns of the TP-MOFs derived from PET powders.

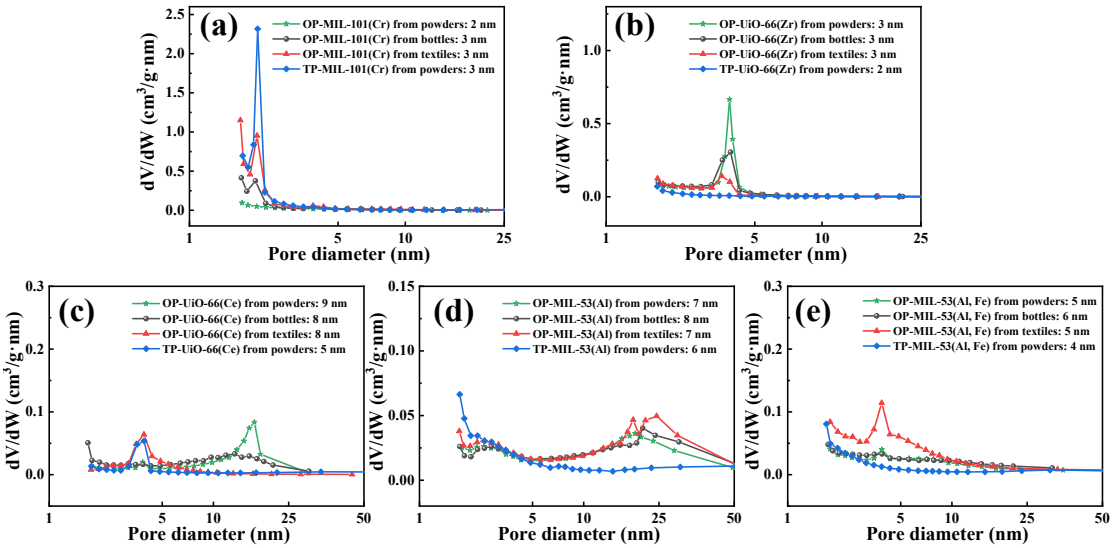

Figure S6. Pore size distributions and mean pore diameters of all MOFs formed.

Table S2. The BET specific surface areas, Zn residues, water adsorptions of the PET-derived MOFs.

MOFs	BET surface area (m^2/g)				Zn content of PET powders-derived MOFs (ppm)	H_2O uptake of PET powders-derived MOFs (mg/g)
	PET powders-derived MOFs	PET bottles-derived MOFs	PET textiles-derived MOFs	conventionally synthesized MOFs		
OP-MIL-101(Cr)	1028.9	990.9	1809.5	2744[1]	488.7	887.2
OP-UiO-66(Zr)	921.6	791.3	647.1	1010[2]	965.1	322.0
OP-UiO-66(Ce)	320.0	361.4	100.5	391[3]	1105.8	227.7
OP-MIL-53(Al)	947.5	789.0	963.3	917[4]	2108.9	706.0
OP-MIL-53(Al, Fe)	894.9	794.5	1413.0	1397[5]	494.9	607.7
TP-MIL-101(Cr)	2591.9			2744[1]		1327.3
TP-UiO-66(Zr)	811.9			1010[2]		215.0
TP-UiO-66(Ce)	504.7	-		391[3]	<235	394.0
TP-MIL-53(Al)	1094.1			917[4]		172.5
TP-MIL-53(Al, Fe)	1093.0			1397[5]		149.0

3. Experimental data for TC photocatalytic removal

The photocatalytic reduction efficiency of the photocatalysts was calculated according to the equation:

$$\text{Removal efficiency}\ (\%) = \frac{(C_0 - C_t)}{C_0} \times 100\% \quad \text{(S6)}$$

where C_0 and C_t refer to the initial concentration of TC and concentration of TC at time t.

The observed reaction rate constants were calculated respectively according to the pseudo-first-order kinetic model (k1, k_{obs}) and pseudo-second-order kinetic model (k_2), as shown in Equations S8-S9.

$$-k_1 t = \ln(\frac{C_t}{C_0}) \quad \text{(S7)}$$

$$k_2 t = \frac{1}{C_t} - \frac{1}{C_0} \quad \text{(S8)}$$

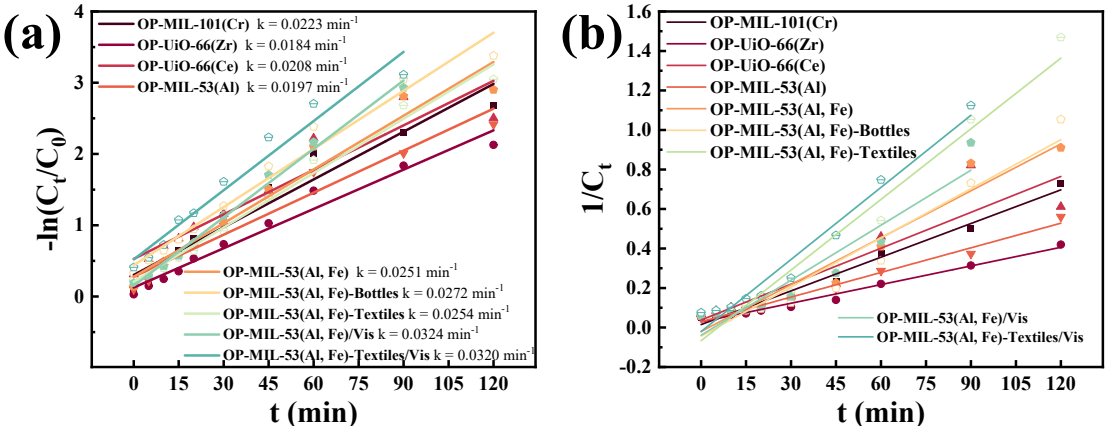

Figure S7. (a) The **pseudo-first-order kinetic curves** and (b) the **pseudo-second-order-kinetic curves** of TC degradation over OP-MOFs derived from PET powders. ($[TC]_0$ = 20 mg/L, 50mL, $[MOF]_0$ = **2 mg**, 25 ℃, 5W UV-light)

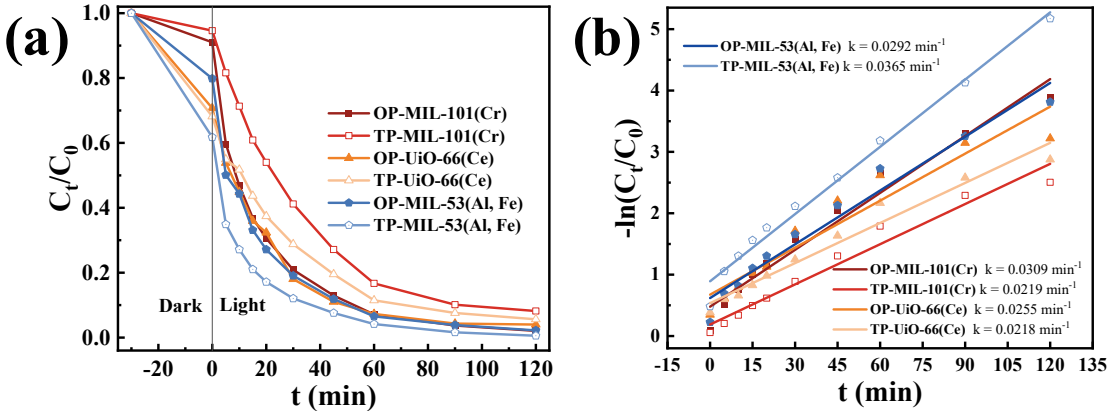

Figure S8. (a) Removal efficiency and (b) the **pseudo-first-order kinetic curves** of TC degradation over MOFs derived from PET powders. ($[MOF]_0$ = **3 mg**, $[TC]_0$ = 20 mg/L, 50mL, 25 ℃, 5W UV-light)

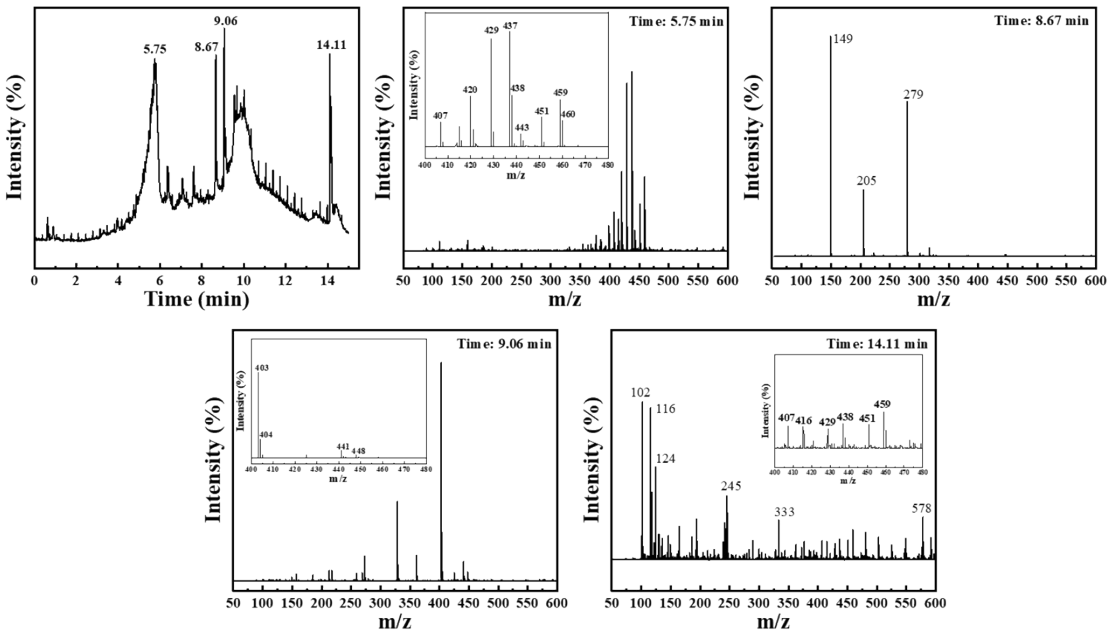

Figure S9. LC-MS of decomposition products of TC photocatalysis for 2 h over OP-MIL-53(Al, Fe).

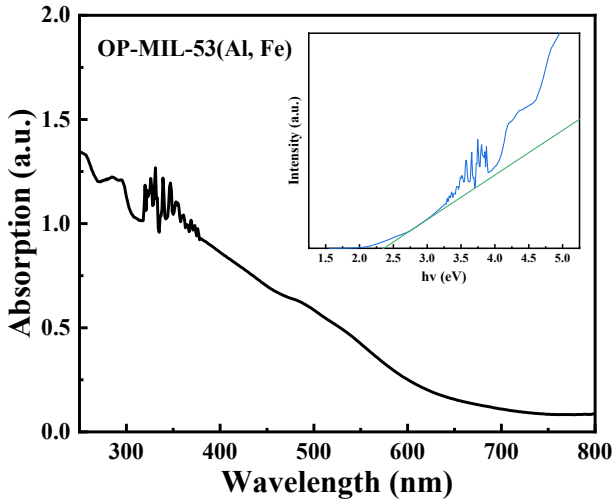

Figure S10. DRS absorbance spectrum for OP-MIL-53(Al, Fe) measured over the range of wavelength 250-800 nm.

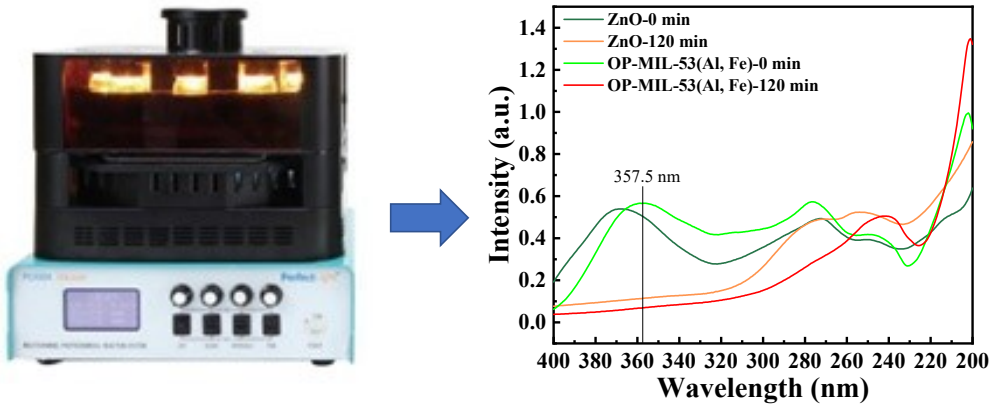

Figure S11. Photocatalytic removal of TC and UV spectra of TC degradation over ZnO and OP-MIL-53(Al, Fe) under 5W UV light ([TC]0 = 20 mg/L, 50mL, m(catalyst) = 2 mg, 25 ℃).

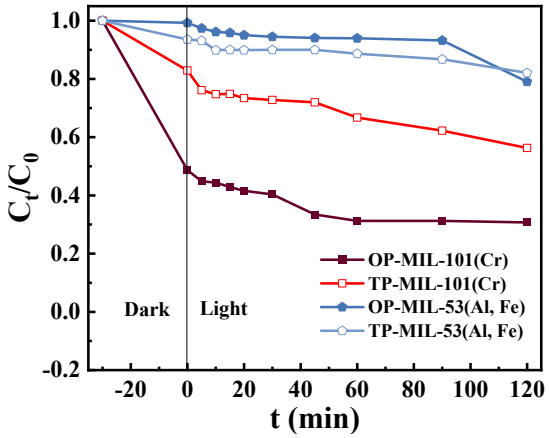

Figure S12. Removal efficiency of **ceftriaxone sodium** degradation over MOFs derived from PET powders. ($[MOF]_0$ = **3 mg**, $[ceftriaxone\ sodium]_0$ = 20 mg/L, 50mL, 25 ℃, 5W UV-light)

Table S3. Kinetic parameters of the adsorption of TC on obtained MOFs.

Catalyst	Pseudo-first-order kinetic model		Pseudo-second-order kinetic model	
	k_1 (mg^{-1})	R^2	k_2 ($g \cdot min^{-1}\ mg^{-1}$)	R^2
OP-MIL-101(Cr)	0.02234	0.94487	0.00568	0.98567
OP-UiO-66(Zr)	0.01839	0.97137	0.00315	0.98408
OP-UiO-66(Ce)	0.02083	0.89943	0.00606	0.84216
OP-MIL-53(Al)	0.01965	0.95572	0.00416	0.98493
OP-MIL-53(Al, Fe)	0.02513	0.96047	0.00791	0.94692
OP-MIL-53(Al, Fe)-Bottles	0.02720	0.97396	0.00829	0.93607
OP-MIL-53(Al, Fe)-Textiles	0.02543	0.98635	0.01192	0.9559
OP-MIL-53(Al, Fe)/Vis	0.03202	0.99409	0.00929	0.90988
OP-MIL-53(Al, Fe)-Textiles/Vis	0.03237	0.96154	0.01217	0.97016

Table S4. Comparison of reported MOF catalysts for the photocatalytic degradation of TC.

Catalyst	System	Mass ratio of cat./TC	TC removal rates, Time	Pseudo-first-order kinetic constant (min^{-1})	Ref.
OP-MIL-53(Al, Fe)	Xe lamp (300 W)	2.0	93.3%, 60min	0.0324	**this work**
OP-MIL-53(Al, Fe)-Textiles	Xe lamp (300 W)	2.0	90.8%, 60min	0.0320	**this work**
TP-MIL-53(Al, Fe)	UV light (5 W)	3.0	95.9%, 60min	0.0365	**this work**
Cu doped MIL-101(Fe)	Xe lamp (300 W)+6 mM PS	2.0 (PS = 6 mM)	94.32%, 120min	0.0321	14
MIL-53(Fe)/bulk g-C_3N_4	Xe lamp (300 W)+60 mM H_2O_2	37.5	100%, 60 min	0.0689	15
MIL-53(Fe, Al)	mercury lamp (500 W)	7.1	94.33%, 50 min	0.1	16
Ni-MOF + CB evaporator	solar+PMS	20	82%, 60 min	0.0115	17
MIL-101(Fe)@MIL-100(Fe)	Xe lamp (300 w)	2.5	80%, 140 min	0.0094	18
g-C_3N_4/PDI@NH_2-MIL-53(Fe)	LED lamp (5 W)+10 mM H_2O_2	8	90%, 60 min	-	19
Fe-MOF	LED lamp (5 W)+3.75 mM H_2O_2	0.36	99.8%, 5min	-	20
Zr-MOF	UV-Vis	50	91.8%, 60 min	0.032	21

References

1 J. Liu, Y. Wei, M. Chang, N. Wang, D. Wang and J.-X. Wang, *AIChE J.*, 2022, **68**, e17522.

2 K. Wang, C. Li, Y. Liang, T. Han, H. Huang, Q. Yang, D. Liu and C. Zhong, *Chem. Eng. J.*, 2016, **289**, 486-493.

3 M. Stawowy, M. Róziewicz, E. Szczepańska, J. Silvestre-Albero, M. Zawadzki, M. Musioł, R. Łuzny, J. Kaczmarczyk, J. Trawczyński and A. Łamacz, *Catalysts*, 2019, **9**, 309-328.

4 C.-X. Yang, H.-B. Ren and X.-P. Yan, *Anal. Chem.*, 2013, **85**, 7441-7446.

5 X. Chen, X. Liu, L. Zhu, X. Tao and X. Wang, *Chemosphere*, 2022, **291**, 133032.

6 M. J. Kang, H. J. Yu, J. Jegal, H. S. Kim and H. G. Cha, *Chem. Eng. J.*, 2020, **398**, 125655.

7 W. Yang, R. Liu, C. Li, Y. Song and C. Hu, *Waste Manage.*, 2021, **135**, 267-274.

8 M. Yan, Y. Yang, F. Chen, D. Hantoko, A. Pariatamby and E. Kanchanatip, *Environ. Sci. Pollut. Res.*, 2023, **30**, 102560-102573.

9 F. Liu, X. Cui, S. Yu, Z. Li and X. Ge, *J. Appl. Polym. Sci.*, 2009, **114**, 3561-3565.

10 P. Pereira, P. E. Savage and C. W. Pester, *ACS Sustain. Chem. Eng.*, 2023, **11**, 7203-7209.

11 C. N. Onwucha, C. O. Ehi-Eromosele, S. O. Ajayi, M. Schaefer, S. Indris and H. Ehrenberg, *Ind. Eng. Chem. Res.*, 2023, **62**, 6378-6385.

12 W. Yang, J. Wang, L. Jiao, Y. Song, C. Li and C. Hu, *Green Chem.*, 2022, **24**, 1362-1372.

13 H. Abedsoltan, I. S. Omodolor, A. C. Alba-Rubio and M. R. Coleman, *Polymer*, 2021, **222**, 123620.

14 L. L. Ma, J. Y. Xu, Y. C. Liu, Y. T. An, Z. C. Pan, B. Yang, L. L. Li, T. Hu and B. Lai, *Sep. Purif. Technol.*, 2023, **305**, 112450.

15 Y. Pan, X. Hu, M. Bao, F. Li, Y. Li and J. Lu, *Sep. Purif. Technol.*, 2021, **279**, 119661.

16 X. Chen, X. Liu, L. Zhu, X. Tao and X. Wang, *Chemosphere*, 2022, **291**,

133032.

17 Z. F. Fan, P. P. He, H. Y. Bai, J. Liu, H. J. Liu, L. J. Liu, R. Niu and J. Gong, *EcoMat*, 2023, **6**, e12422.

18 Y. N. Jin, X. C. Mi, J. L. Qian, N. Ma and W. Dai, *ACS Appl. Mater. Inter.*, 2022, **14**, 48285-48295.

19 Y. Y. Li, Y. Fang, Z. L. Cao, N. J. Li, D. Y. Chen, Q. F. Xu and J. M. Lu, *Appl. Catal. B: Environ.*, 2019, **250**, 150-162.

20 P. D. Liu, Y. Chen, Liu, AG, Z. T. Chen and B. Li, *J. Mat. Chem. A*, 2023, **11,** 25322-25331.

21 S. P. Tripathy, S. Subudhi, A. Ray, P. Behera, J. Panda, S. Dash and K. Parida, *J. Colloid Interf. Sci.*, 2023, **629**, 705-718.